THE JOURNAL OF PHYSICAL CHEMISTRY B

ARTICLE

pubs.acs.org/JPCB

Stability and Instability of the Isoelectronic UO_2^{2+} and PaO_2^{+} Actinyl Oxo-Cations in Aqueous Solution from Density Functional Theory Based Molecular Dynamics

Riccardo Spezia,[*,†] Bertrand Siboulet,[‡] Sacha Abadie,[†,§] Rodolphe Vuilleumier,[§] and Pierre Vitorge[*,†,⊥]

[†]Laboratoire Analyse et Modélisation pour la Biologie et l'Environnement, UMR 8587, CNRS, CEA, UEVE, Université d'Evry Val d'Essonne, Boulevard F. Mitterrand, F-91025 Evry Cedex, France

[‡]CEA, DEN, DRCP, F-30207 Bagnols-sur-Cèze, France

[§]Ecole Normale Supérieure, Département de Chimie, 24, rue Lhomond, 75005 Paris, France, and UPMC Univ Paris 06, 4, Place Jussieu, 75005 Paris, UMR 8640 CNRS-ENS-UPMC, France

[⊥]CEA, DEN, Laboratoire de Spéciation des Radionucléides et des Molécules, F-91991 Gif-sur-Yvette, France

ABSTRACT: In this work, Pa(V) monocations have been studied in liquid water by means of density functinal theory (DFT) based molecular dynamic simulations (CPMD) and compared with their U(VI) isoelectronic counterparts to understand the peculiar chemical behavior of Pa(V) in aqueous solution. Four different Pa(V) monocationic isomers appear to be stable in liquid water from our simulations: $[PaO_2(H_2O)_5]^+$(aq), $[Pa(OH)_4(H_2O)_2]^+$(aq), $[PaO(OH)_2(H_2O)_4]^+$(aq), and $[Pa(OH)_4(H_2O)_3]^+$(aq). On the other hand, in the case of U(VI) only the uranyl, $[UO_2(H_2O)_5]_2^{+}$(aq), is stable. The other species containing hydroxyl groups replacing one or two oxo bonds are readily converted to uranyl. The Pa−OH bond is stable, while it is suddenly broken in U−OH. This makes possible the formation of a broad variety of Pa(V) species in water and participates to its unique chemical behavior in aqueous solution. Further, the two actinyl oxocations in water are different in the ability of the oxygen atoms to form stable and extended H-bond networks for Pa(V) contrary to U(VI). In particular, protactinyl is found to have between 2 and 3 hydrogen bonds per oxygen atom while uranyl has between zero and one.

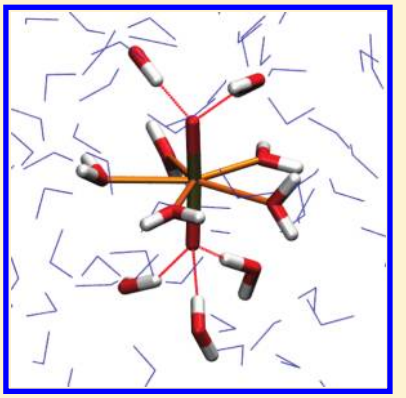

1. INTRODUCTION

Actinyl ions (linear $AnO_2^{(z-4)+}$) are central to the chemistry of most of the actinide (An) elements in high oxidation states (z = +5 and +6), namely for uranyl (An = U) and trans-uranyl (An = Np, Pu, Am) ions.[1−3] They are ubiquitous in most An(V) and An(VI) complexes or compounds. This reflects the chemical stability of the actinyl linear skeleton, while the ligands remain in the equatorial plane of $AnO_2^{(z-4)+}$. The uranyl linear skeleton is usually only slightly destabilized by equatorial ligands;[4] thus, $AnO_2^{(z-4)+}$ ions are considered as quite hard cations with respect to equatorial interactions.

AnO_2^{2+} cations are observed for U and the An = Np, Pu, and Am transuranic elements. They have the same geometries, and similar chemical behaviors toward hard electronegative ligands. This results from the fact that the covalent actinyl linear skeleton of AnO_2^{2+} is the same in all these actinyl ions (AnO_2^{2+}) despite not being isoelectronic. The additional electrons in transuranics—as compared to U—are localized on the f-orbitals that do not generally participate in bonding and, therefore, do not alter the actinyl covalent linear skeleton. AnO_2^{2+}(aq) is typically the dominating species of An(VI) in acidic solutions, and the equatorial water ligands are hydrolyzed in aqueous solutions at about the same pH for all actinyls presented here ($pH_{1/2}$ is in the range 5.2−5.5).[5] Note that AnO_2^{2+} with An = Np, Pu, and Am transuranian elements have analogous hydrolyzing properties.[2,3]

Among the An oxocations, uranyl (UO_2^{2+}) is the most well-known. An excellent review by Grenthe et al. provides reliable stoichiometries and stabilities of its aqueous complexes as obtained from experimental studies.[2] Uranyl hydration has also been studied by theoretical methods.[6−15] The most stable oxidation state for uranium in the uranyl ion is U^{6+} where uranium has the Rn electronic configuration.

For the An(V) cations, uranium and transuranics are chemical analogues. AnO_2^{+}(aq) is the dominating species of the U(V) and transuranic An(V) cations in aqueous solutions. These monocations are less easily hydrolyzed ($pH_{1/2} = 11.3 \pm 0.7$)[3,5] than the AnO_2^{2+}-(aq) dications ($pH_{1/2}$ in the range 5.2−5.5) as expected from the differences in their charges, recalling that all the AnO_2^{+}(aq) cations are hydrolyzed at about the same pH ($pH_{1/2} = 11.3 \pm 0.7$).

The An(V) series formally starts with Pa. It is the element just before U in the periodic table. Pa(V) and U(VI) are isoelectronic and PaO_2^{+} and UO_2^{2+} indeed have similar electronic

Received: December 9, 2010
Revised: February 18, 2011
Published: March 16, 2011

configurations.[16] Pa is the first actinoid easily oxidized to the +5 oxidation state, its more stable oxidation state. Intriguingly, Pa(V) is not really a chemical analogue to any other An(V).[17] In the monocationic series of An(V) hard cations, the UO_2^+, NpO_2^+, PuO_2^+, and AmO_2^+ are chemical analogues.[3] The first one, PaO_2^+, is a chemical exception among the series, as typically seen in hydrolysis.[17]

Using similarities between molecules or ions is a typical approach to understanding their chemical properties.[1−3,5,18] F-block elements are usually chemical analogues of one another when in the same oxidation state, since they form cations of the same charges and similar sizes giving similar electrostatic interactions with a given ligand. This relationship is believed to be due to the hard character of the An ions. On the other hand, the high stability of $AnO_2^{(z-4)+}$ is due to the strong An-O_{yl} actinyl triple bonds. In that case analogous behavior is expected between isoelectronic species.

Pa(V) hydrolysis experimental raw data were recently re-examined.[19,20] Unfortunately, the number of water molecules cannot be determined via experimental hydrolysis studies. The Pa(V) aqueous monocation can be a mixture of PaO_2^+, $PaO(OH)_2^+$, or $Pa(OH)_4^+$. The total stoichiometries differ only by the number of water molecules and are actually isomers in liquid water. These possible different structures of Pa(V) in water can be related to the tendency toward sorption on any solid support material.[21−23] Since protactinium will be produced in thorium fuel reactors that are under consideration for long-term energy production, the understanding of its in water behavior at a molecular level is important to rationalize the nuclear fuel management, including radioactive wastes containing Pa.

The structure of the Pa(V) monocation is not completely understood in noncomplexing aqueous solutions.[20,24] Little experimental structural data has been published. The PaO_2^+ stoichiometry—and even PaO_2^{2+}—has been detected in the gas phase,[25] but to our best knowledge, the characteristic linear protactinyl (PaO_2^+) geometry has never been observed in the condensed phase. This difference between Pa(V) and trans-protactinics (V), along with their different hydrolysis properties, has been thought to suggest some instability of PaO_2^+.[20]

Extended X-ray absorption fine structure (EXAFS) studies are published for Pa(V) in acidic (sulfate) aqueous solutions providing a Pa−O distance of 1.79 Å that is interpreted as evidence of PaO^{3+} inside the sulfate complex.[26] Recently, a similar (1.75 Å) short distance was found in an analogous EXAFS study in oxalate aqueous solutions.[27] However, as indicated by the authors, their quantum chemistry calculations show a significantly longer Pa−O_{yl} distance (1.89 Å) than that observed by EXAFS (1.75 Å). Indeed, the 0.16 Å difference is about three times the expected accuracy of both EXAFS and density functional theory (DFT). This can be attributed to the formation of PaO^{3+}. This species is also proposed to form in some experimental results performed in concentrated noncomplexing acidic solutions;[17,19] DFT calculations indicate that both PaO^{3+}(aq) and $Pa(OH)_2^{3+}$(aq) could very well be of similar thermodynamic stabilities.[24]

A pleasing explanation was recently proposed for the puzzling chemical behavior of Pa(V). It is proposed that PaO_2^+(aq) is not the only possible Pa(V) hydrated monocation[20,24] resulting from some destabilization of PaO_2^+. Toraishi et al. made a detailed comparison of the orbitals for several isoelectronic Pa(V) and U(VI) oxo-hydroxo-cations with a first hydration layer plus a dielectric continuum to mimic bulk solvent effects.[24] Siboulet et al. used water clusters of Pa with two hydration layers allowing some description of apical hydration, namely hydrogen bonding on the O_{yl} atoms. They also optimized geometries with two additional hydration layers for the PaO_2^+(aq), $PaO(OH)_2^+$(aq), and $Pa(OH)_4^+$(aq) isomers providing evidence of new covalent bonding around Pa(V).[20] Furthermore, they found that Pa−O_{yl} bonds are triple bonds as in U(VI), while the Pa−O_{hydr} are usually double bonds in Pa(V) oxo-hydroxo-cations. They also show that there is some intrinsic instability of the PaO_2^+ covalent skeleton as compared to the isoelectronic UO_2^{2+} one. Both studies propose that this instability is correlated to more negative partial atomic charges on the O_{yl} atoms of PaO_2^+ as opposed to the corresponding of UO_2^{2+} O_{yl} atoms as calculated by the Mulliken[24] or NBO[20] method. In line with this explanation, Siboulet et al. proposed that the O_{yl} oxygen atoms are more easily protonated—or equivalently more alkaline—in PaO_2^+ than in UO_2^{2+}, such protonations are suggested by the short (1.55 Å) apical hydrogen bonds in $PaO_2(H_2O)_5(H_2O)_{10}(H_2O)_6^+$ clusters in comparison with (1.92 Å) the UO_2^{2+} isoelectronic cluster.

Water molecules in apical position have been obtained in optimized uranyl−water clusters[15] as well as from other DFT calculations of hydrated clusters.[28] Water molecules hydrogen bonded to the O_{yl} atoms were also found by earlier molecular dynamic (MD) simulations performed with an empirical and nonpolarizable force field.[29] Five water molecules were found in the equatorial plane at a distance that agrees well with experiments. New MD simulations of UO_2^{2+} in liquid water were recently reported: one based on a NEMO force field parametrized to reproduce high level (CASPT2) ab initio calculations,[30] two are DFT-based studies,[31,32] and one uses a mixed Hartree−Fock/molecular mechanics approach.[33] These simulations are in agreement with experimental U−O distances.[34,35] The results suggest that the apical water molecule interaction with uranyl is very weak, and no structured hydrogen-bond network is formed around the U O_{yl} atoms.

We present here the study of isoelectronic PaO_2^+ and UO_2^{2+} by DFT-based MD in liquid water in order to compare their hydration properties. Of particular interest will be the difference in the interactions between O_{yl} atoms and surrounding water molecules since they have been suggested—from static calculations—to have an important role in the Pa(V) chemical exception.[20] Note that it was shown that DFT is not always able to correctly treat NpO_2^{3+} and PuO_2^{4+} in the gas phase[16] but is able to obtain correct geometries of molecules containing Np(VII) if a proper basis set is used.[36] Thus the present study makes a comparison between Pa(V) and U(VI) where DFT is known to provide a correct description; however, treating iso-electronic trans-uranium oxocations via DFT-based dynamics will need further developments in DFT theory.

In the past few years, DFT-based MD was shown to be able to study hydration of several metal cations.[37−45] Recently, this approach has been extended to very heavy metal cations like uranyl,[7,31,32] La(III),[46] Gd(III),[47,48] and Po(IV),[49] and the behavior of these species was studied in water. Structural properties, hydrolysis, and connections between electronic structure and solvation behavior were able to be described.

In the present work, we use DFT-based MD within the Car−Parrinello (CPMD) framework[50] to study the Pa(V) hydrated monocations, PaO_2^+, $PaO(OH)_2^+$, and $Pa(OH)_4^+$ and make systematic comparisons with their isoelectronic U(VI) counterparts.

The outline of the remainder of this paper is as follows. In section 2, we present the methods employed including a description of the systems studied (2.1), the way we have generated and tested the Pa pseudopotential (2.2), and the

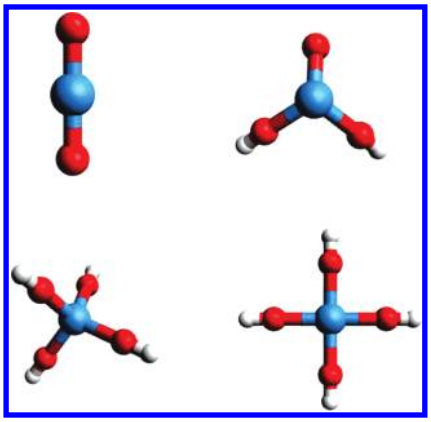

Figure 1. Structure of Pa(V) species studied (from top to bottom and from left to right): PaO_2^+, $PaO(OH)_2^+$ (here the minimum gas phase energy structure), $Pa(OH)_4^+$ in T_d symmetry and $Pa(OH)_4^+$ in D_{4h} symmetry. Bulk water molecules are not shown for simplicity. The same geometries were considered changing the central Pa(V) with U(VI).

details on the MD simulation procedure (2.3). In section 3, we show results and briefly discuss them. First, we discuss the stability of the various systems studied (3.1), then the hydration structure that Pa(V) species assume in liquid water (3.2), and finally the nature of Pa(V) and U(VI) oxocations interaction with surrounding water molecules (3.3). Section 4 summarizes and concludes the work.

2. METHODS

2.1. Systems Studied. In order to understand Pa(V) behavior in liquid water, we have studied different possible forms of Pa(V) in acidic conditions: the oxocation, protactinyl, PaO_2^+ (isoelectronic to uranyl), the mono-oxocation, $PaO(OH)_2^+$—formally $PaO_2^+ + H_2O$—and $Pa(OH)_4^+$—formally $PaO(OH)_2^+ + H_2O$. The structure of $Pa(OH)_4^+$, as already reported,[20] can be present in two forms: (i) distorted octahedral, where four sites are occupied by OH^- and the two remaining by two water molecules (labeled D_{4h}), and (ii) tetrahedral (labeled T_d). Note that D_{4h} and T_d symmetries have been pointed out also in the gas phase structures of $[U^{(VI)}O_4]^{2-}$ and $[Np^{(VII)}O_4]^-$, respectively.[36] In Figure 1, we show these structures. All these systems were immerged in bulk water, mimicked by employing standard periodic boundary conditions (PBC). The systems are composed of the Pa(V) containing solute and 122, 121, and 120 solvent water molecules for PaO_2^+, $PaO(OH)_2^+$, and $Pa(OH)_4^+$ respectively. Analogous systems were built for U(VI), namely the oxocation uranyl, UO_2^{2+}, the mono-oxocation, $UO(OH)_2^{2+}$, and the hydroxide, $U(OH)_4^{2+}$, with both structures, D_{4h} and T_d.

2.2. Pa Pseudopotential Development. DFT-based molecular dynamics within the Car−Parrinello scheme, CPMD, employs plane-waves (PWs) to express system's electronic wave function. In this PW representation, only valence electrons are treated explicitly since a computationally reliable PW cutoff is used. In order to do so, pseudopotentials (PPs) are employed. Electrons are separated into two groups: valence electrons that are explicitly treated and core electrons that are taken into account by the PP. We used standard Troullier−Martins PPs.[51] The O and H valence/core partition is well studied, and the parameters have been previously obtained. For U, we used the PP recipe presented by Bühl and co-workers,[31] which has been successfully employed to study uranyl hydration.

For Pa, we developed a semicore Troullier−Martins PP as follows. The reference configuration used to generate the PP for Pa was Pa^{2+}: $[Rn]5f^26d^17s^0$. The orbitals 6s, 6p, 6d, and 5f were include in the PP with cutoffs of 1.34, 1.59, 2.31, and 1.09 au, respectively. When using this PP with PWs, the semilocal Kleinman−Bylander form was used with the p channel as the local channel.[52]

We checked the validity of our Pa PW-PP by optimizing geometries of small Pa−O clusters and comparing geometries with previously reported calculations.[20] The PP that is able to give results in good agreement with other calculations providing reliable results on small systems is, often, also able to correctly address several systems containing this atom. We have recently used this approach for cobalt,[53−56] lanthanum,[46] and polonium.[49] In the present case, the PP also needs to be used for Pa when using Gaussian atomic centered basis sets (GBS), since it is a very heavy element, and core electrons need an effective core potential (ECP) to be treated correctly. Fortunately, much work has been done in the literature to setup effective core potential for actinides. We used the same ECP and GBS used previously by Siboulet et al.,[20] namely a "small-core" quasi-relativistic ECP where the "semi-core" 5s, 5p, and 5d electrons are treated explicitly.[57] The (11s, 10p, 10d, 7f) basis set associated with the ECP was flexibly contracted to [8s, 7p, 7d, 4f] as previously reported.[57] We also used a PP for oxygen atoms with a "double-ζ plus polarisation plus diffuse" (DZP+) basis sets (5s, 5p, 1d) contracted to [3s, 3p, 1d] to describe the valence electrons.[58] A standard double-ζ basis set is used for hydrogen.[59] We used the B3LYP functional[60] as a reliable reference to validate our PW-PP, since it provides accurate geometries for UO_2^{2+}[13−15] and PaO_2^+[20,24] hydrations in clusters. The BLYP functional[61−63] with the same GBS and ECP was also used to compare with PW-PP/BLYP results.

In Table 1, we show the geometrical parameters of small ions containing Pa(V) obtained in geometry optimizations with our developed PW-PP and the BLYP functional as well as with the GBS results using both BLYP and B3LYP. The PW-PP results are in agreement with the GBS ones, and interestingly, they are closer to the GBS B3LYP results than to the GBS BLYP ones providing further confidence in our PW-PP. For $PaO(OH)_2^+$

Table 1. Pa−O Distances (Å) for Different Systems in the Gas Phase Calculated at BLYP/PW-PP, BLYP/GBS, and B3LYP/GBS Levels of Theory

system	bond	BLYP/PW-PP	BLYP/GBS	B3LYP/GBS
PaO_2^+				
	Pa−O	1.794	1.801	1.778
$PaO(OH)_2^+$ (planar)				
	Pa−O	1.808	1.826	1.798
	Pa−O(H)	2.053	2.062	2.044
$PaO(OH)_2^+$ (C_s)				
	Pa−O	1.817	1.828	1.804
	Pa−O(H)	2.043	2.054	2.038
$Pa(OH)_4^+$ (T_d)				
	Pa−O(H)	2.053	2.066	2.043
$Pa(OH)_4^+$ (D_{4h})				
	Pa−O(H)	2.058	2.062	2.047

Table 2. Energy Differences (kcal/mol) of $PaO(OH)_2^+$ and $Pa(OH)_4^+$ in the Gas Phase Calculated at BLYP/PW-PP, BLYP/GBS, and B3LYP/GBS Levels of Theory

ΔE	BLYP/PW-PP	BLYP/GBS	B3LYP/GBS
$E[PaO(OH)_2^+/plan] - E[PaO(OH)_2^+/C_s]$	1.534	1.786	1.592
$E[Pa(OH)_4^+/D_{4h}] - E[Pa(OH)_4^+/T_d]$	18.214	15.400	17.155

and $Pa(OH)_4^+$, we have studied two isomers: planar versus C_s and T_d versus D_{4h}, respectively. Also in that case energy differences obtained with our developed PW-PP are in agreement with the GBS ones (see Table 2).

We used our previously published clusters[20] to build initial geometries. All PW-PP/BLYP calculations are done with CPMD[64] while GBS/B3LYP and GBS/BLYP with Gaussian03.[65]

2.3. Simulation Procedure. For each system, the total number of oxygen atoms was set to 124. For example, in $AnO_2^{(z-4)+}$ ($z = 5$ for Pa and $z = 6$ for U), we have 122 water molecules around the central ion, while there are 121 for $AnO(OH)_2^{(z-4)+}$ and 120 for $An(OH)_4^{(z-4)+}$. PBC are used in all cases to mimic the liquid phase. A DFT-based MD was used with the BLYP functional. The cutoff value for the plane-waves was set to 90 Ry.

The fictious mass of the electronic wave function has been chosen at 400 au with a time step to numerically integrate motion equation of 4 au (= 0.0967 fs). All the systems were previously equilibrated for 100 ps via classical molecular dynamics where the solute was kept rigid and only water molecules were allowed to equilibrate at 300 K. The box dimension was adjusted in order to obtain the correct water density at 300 K. Finally, the box length was then set to 15.3909 Å for each edge. Then CPMD simulations were generated, and after 1 ps of equilibration, we obtained equilibrated trajectories for about 13 ps. The full length was obtained for Pa(V) systems and UO_2^{2+} since, as we will describe in much detail in section 3, other U(VI) species are instable and quickly transformed back to UO_2^{2+}.

Structural analyses of the hydration patterns were done using standard radial distribution functions (RDFs) and coordination numbers (CNs). CNs are obtained through the integration of corresponding RDFs between r_{min} and r_{max}. For the first shell CN (CN_1), $r_{min} = 0$ and r_{max} corresponds to the first minimum of the radial distribution function (RDF). Furthermore, $r_{min} = r_{max}$ is used for CN_1 and r_{max} corresponds to the second minimum of RDF for second shell CN (CN_2). Radial distribution functions are complemented by angular distribution functions: (i) the O−Pa−O (and O−U−O) angle formed by the actinide and two oxygen atoms from its first hydration shell, (ii) the tilting angle formed by the Pa−O (and U−O) vector and the plane defined by the water molecule in the first hydration shell, and (iii) the θ angle formed by the Pa−O (and U−O) vector (O of the first hydration shell) and the vector sum of the two O−H bonds (of water in first hydration shell). For a graphical explanation, one can see Figure 4 of ref 46.

3. RESULTS AND DISCUSSION

3.1. Pa(V) versus U(VI) Stability. We have considered four starting systems for both Pa(V) and U(VI). We pair the isoelectronic ions of same geometry: (**I**) PaO_2^+ and UO_2^{2+}; (**II**) $PaO(OH)_2^+$ and $UO(OH)_2^{2+}$; (**III**) $Pa(OH)_4^+$ and $U(OH)_4^{2+}$ where OH^- are in a plane and the shell is fulfilled by two water molecules. We call for simplicity these systems with their symmetry point group, D_{4h}, that is the symmetry of the initial structure and that is lost in the dynamics where any symmetry constrain is employed. (**IV**) $Pa(OH)_4^+$ and $U(OH)_4^{2+}$ have OH^- groups in a tetrahedral arrangement, and we call this structure T_d; albeit, as we will see in the following, in solution the tetrahedral symmetry is quickly lost. The actinyl ($AnO_2^{(z-4)+}$) dioxo-cations (system **I** in our notations) were found to be stable in solution for both Pa(V) and U(VI) as expected. The $AnO(OH)_2^{(z-4)+}$ oxo-hydroxo-cation (system **II**) is stable for Pa(V), while it is not for U(VI): a proton of one of the two OH^- groups surrounding U(VI) is transferred to a neighbor (second sphere) water molecule ($U-O-H\cdots OH_2 \rightarrow U-O\cdots H-OH_2$) within about 100 fs. As a result, a uranyl moiety is formed corresponding to the reaction $UO(OH)_2^{2+} + H_2O \rightarrow UO_2OH^+ + H_3O^+$ that gives the usual uranyl ion here hydrolyzed in its equatorial plane.

The same holds for the $An(OH)_4^{(z-4)+}$ hydroxo-cations (systems **III** and **IV**). The Pa(V) ones are stable, while a proton transfer quickly occurs from an OH^- group being around U(VI) and a water molecule of the second hydration layer. A coordinated OH^- ligand looses a proton thus forming an UO oxo bond; however, in this case the process is slower (in 600 and 770 fs for systems **III** and **IV**, respectively) and leads to U(VI) with one oxygen and three OH^-: $U(OH)_4^{2+} + H_2O \rightarrow [UO(OH)_3^+] + H_3O^+$. This structure is not stable, and it looses another proton after a relatively short time (about 600 and 2000 fs, respectively). Specifically, the proton lost is the one in the opposite position with respect to the UO bond, forming uranyl twice hydrolyzed in its equatorial plane:[66−70] $[UO(OH)_3^+] + H_2O \rightarrow UO_2(OH)_2 + H_3O^+$. Note that all these reactions are not intended to be at equilibrium. They simply give us the tendency of the different species to be stable as for systems **I** of U(VI) and Pa(V) and **II**, **III**, and **IV** of Pa(V) or instable, as seen for systems **II**, **III**, and **IV** of U(VI).

A clear difference is thus underlined between the Pa(V) and U(VI) isoelectronic structures under the same conditions.[71] While Pa(V) is able to form a large variety of structures in water, all the U(VI) initial geometries tested strongly tend to form uranyl. This, as discussed in the following, could be a reason why Pa(V) behaves so differently in water with respect to U(VI) and other *trans*-actinide oxocations. Note also that our results are in agreement with previously reported calculations showing that U−O bonds are stronger than Pa−O bonds, due to the different contribution of 5f and 6d orbitals of the actinide.[24] In U(VI) the 5f orbitals play an important role in the bonding while for Pa(V) the 6d orbitals are more involved. The stronger $U-O_{oxo}$ bonding is associated with more charge transfer from the O_{oxo} lone pair to the U−O covalent triple bond corresponding to less negative atomic charge as already published[20,24] and virtually no H-bond network about the uranyl O_{oxo} as evidenced in the present study.

All the Pa(V) structures are stable with similar Kohn−Sham energies. Looking into the details of the T_d simulation, we notice that the initial tetrahedral arrangement of the four OH^- groups around Pa is lost in the initial portion of the trajectory. In Figure 2, we report O−Pa−O angle trajectories of T_d and D_{4h} simulations to show how the initial T_d symmetry is lost and the

dx.doi.org/10.1021/jp111726b |J. Phys. Chem. B 2011, 115, 3560–3570

OH^- are arranged in a way that is similar to the D_{4h}. On the other hand, the D_{4h} simulation keeps its structure during the whole simulation. As we will see in the following, the difference comes from a different number of water molecules in the first shell.

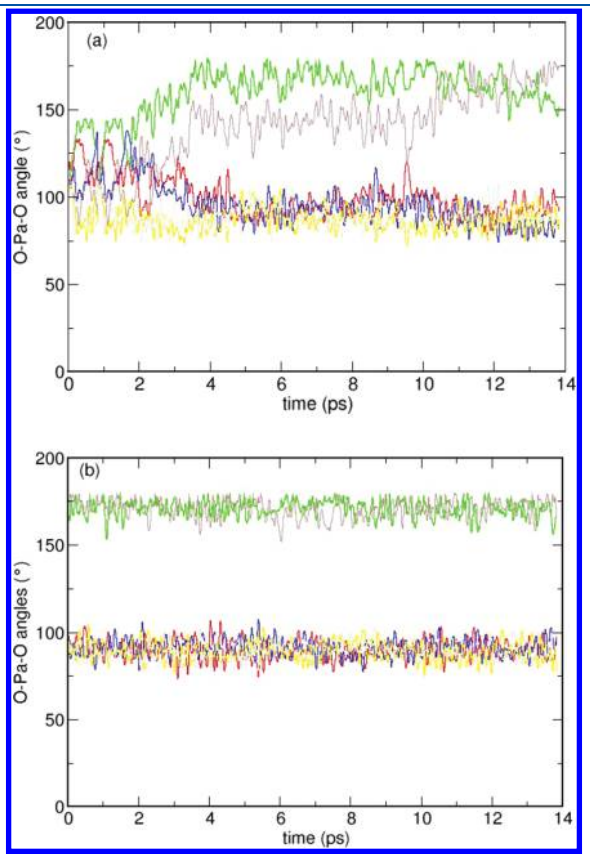

Figure 2. O—Pa—O angle trajectories for T_d (a) and D_{4h} (b) simulations.

3.2. Pa(V) versus U(VI) First Coordination Shells. All the Pa(V) species studied are chemically stable (in Figure 3, we show snapshots from Pa(V) CPMD simulations in liquid water), i.e. each PaO_{yl} bond is maintained through the full simulation length. The same holds for OH^- groups that are stable since we observe neither migration apart in the first Pa(V) shell nor proton transfer to or from surrounding water molecules. For each species we discuss different hydration structures in the following. Table 3 summarizes structural properties reporting Pa—O radial distribution function (RDF) peaks and associated coordination numbers. In the same table, we report the same properties obtained for UO_2^{2+}. Note that these results are in agreement with previously reported DFT-based MD simulations[31] and experiments.[35] Since the Pa PW-PP was built in a similar fashion and was successfully tested versus BLYP and B3LYP calculations

Table 3. Structural Properties of Oxygen Distribution around Pa(V) and U(VI) Stable Species[a]

	r_1	CN_1	$r_{1.5}$	$CN_{1.5}$	r_2	CN_2
UO_2^{2+}	1.81	2			2.41	5
PaO_2^+	1.93	2			2.51	5
$PaO(OH)_2^+$	1.92	1	2.16	2	2.50	4
$Pa(OH)_4^+$ (D_{4h})	2.11	4			2.35	2
$Pa(OH)_4^+$ (T_d)	2.14	4			2.51	3
UO_2^{2+}/exp from ref 35	1.76	2			2.41	5

[a] Here, r_1 and CN_1 for PaO_2^+, $PaO(OH)_2^+$, and UO_2^{2+} correspond to O_{yl} atoms, while for $Pa(OH)_4^+$ species, they correspond to hydroxyl oxygen atoms. Also, $r_{1.5}$ and $CN_{1.5}$ correspond to O_{hydr} atoms of $PaO(OH)_2^+$; r_2 and CN_2 correspond to O_w atoms.

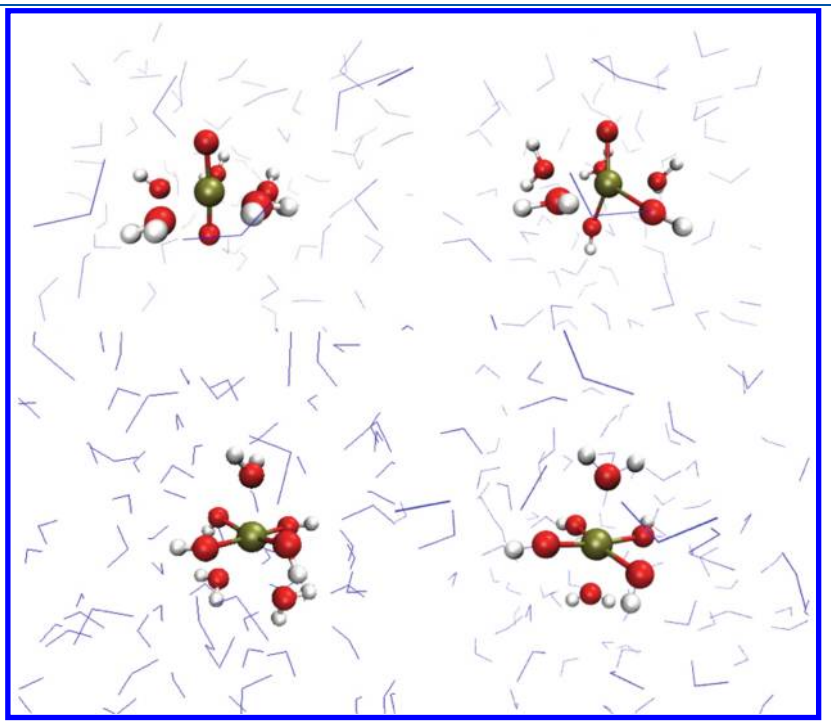

Figure 3. Snapshots of Pa(V) CPMD simulations (from top to bottom and from left to right): PaO_2^+, $PaO(OH)_2^+$, $Pa(OH)_4^+/T_d$ and $Pa(OH)_4^+/D_{4h}$. Pa is in yellow, O is in red, and H is in white. Bulk water molecules (from second hydration shell) are in blue lines.

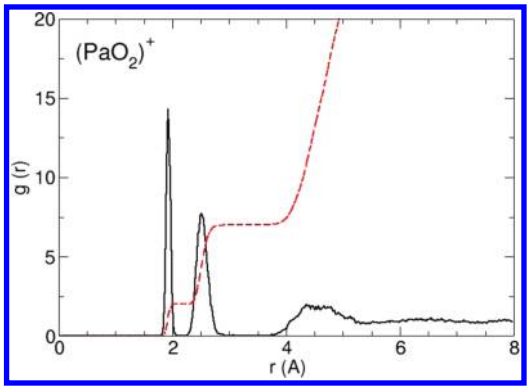

Figure 4. Pa−O radial distribution function, $g(r)$, for the PaO_2^+ simulation. The dashed line shows the integrated CN.

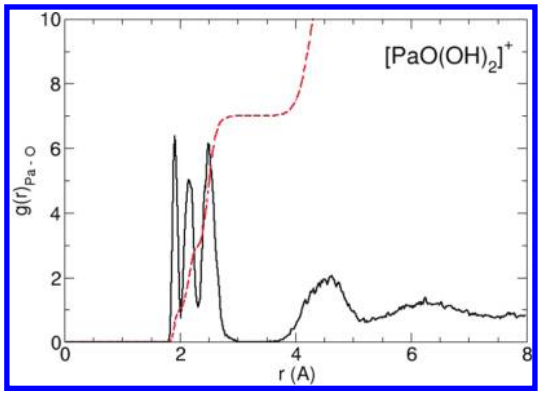

Figure 5. Pa−O radial distribution function, $g(r)$, for the $PaO(OH)_2^+$ simulation. The dashed line shows the integrated CN.

on small clusters, we have confidence in its performance on Pa(V) hydration patterns, even though to our best knowledge no structural data are available in noncomplexing aqueous solution.

In the case of PaO_2^+, we have two oxygen atoms at 1.93 Å corresponding to the first peak of the Pa−O RDF, shown in Figure 4 (these are the O_{yl} atoms). Five water molecules hydrate Pa(V) at about 2.51 Å. They are placed in equatorial positions, as for uranyl in water. These 1.93 and 2.51 Å Pa−O distances compare well with that obtained from static DFT/B3LYP calculations: 1.86 and 2.59 Å for $PaO_2(H_2O)_5^+$ in the gas phase[24] and 1.89 and 2.53 Å adding a second hydration sphere including apical water molecules.[20] Comparing protactinyl with uranyl, we found that, in parallel to what was found in the gas phase, the PaO bond is longer than the UO bond by 0.12 Å from our CPMD simulations in liquid water (Table 3). A difference of 0.07 Å is obtained in the gas phase,[16,16,20] and one of 0.09 Å is in clusters with two hydration layers.[15,20] This trend might be interpreted as a progressive destabilization of PaO_2^+ by increasing hydration that does not occur for UO_2^{2+}. The five water molecules in the equatorial plane are at a shorter distance for UO_2^{2+} than for PaO_2^+, of about 0.1 Å, that reflects also the differences in ionic radii of about 0.05 Å between U(VI) and Pa(V).[72]

The RDF also shows that the different shells are well separated without any interchanging between them in the accessible simulation time-length.

In the case of $PaO(OH)_2^+$, we have only one Pa−O bond at a distance (1.92 Å) that is almost the same as that in PaO_2^+ (1.93 Å), thus much larger than that tentatively attributed to the PaO^{3+} group (in the range 1.75−1.79 Å from EXAFS in complexing media[26,27]). The two oxygen atoms of the OH groups (O_{hydr}) are only 0.24 Å further, and water molecules are at a distance of 2.50 Å, similar to that of PaO_2^+ equatorial water molecules. But in this case, unlike from PaO_2^+, we have only four equatorial water molecules, since one O_{yl} and two O_{hydr} atoms (for a total of three oxygen atoms) have a bigger steric hindrance around Pa(V) than the two O_{yl} atoms of protactinyl. The total number of oxygen atoms in this case is seven. From the RDF of Figure 5, we can see the three peaks corresponding to O_{yl}, O_{hydr}, and oxygen atoms of water, O_w, (r_1, $r_{1.5}$, and r_2, respectively, in Table 3). The peaks are not separated, but this does not correspond to any exchange mechanism taking place. Simply, the three peaks partially overlap due to thermal fluctuations. Other water molecules in further hydration shells are well separated, and we do not see any interchanging with them in the time-length of our simulations. Inspecting this simulation in more detail, we notice that the two O_{hydr} atoms are not equivalent, as shown in Figure 6. One is almost linear with O_{yl}—in a trans-like position—but still bearing its proton, while the other one forms an angle not far from 90°. As we already remarked from the total Pa−O RDF, we have a unique peak corresponding to Pa−O_{hydr}. If we separately monitor the two distances, one is shorter than the other one by about 0.1 Å even if the two distributions largely overlap. Furthermore, the shortest Pa−O_{hydr} distance (the distribution peak being at about 2.12 Å) is not as short as a Pa−O_{yl} one (about 1.92 Å). The overlap of the two distributions due to thermal fluctuations does not allow the clear identification of this difference from global Pa−O RDF such that it will be difficult to separate the two contributions from structural experimental data. Nevertheless, this is in line with the suggestion coming from gas phase calculations[20] that a "protonated protactinyl" is another possible species. We should note that the starting structure is a symmetric one where the two Pa−O_{hydr} bonds are initially equivalent, and the system spontaneously changes into a nonsymmetric structure.

Finally, we study $Pa(OH)_4^+$ hydration by using two starting structures, D_{4h} and T_d, as described before. In Figure 7, we show the Pa−O RDF of both simulations. In the case of the D_{4h} structure, the four O_{hydr} groups are at shorter distances than in the T_d system. As we have previously discussed, the D_{4h} system is composed of four O_{hydr} in a plane and two water molecules in the remaining elongated distorted octahedral positions resulting in a Pa CN of 6. This 4 + 2 structure is maintained in the simulation, and it is very stable as shown by the narrow RDF first peak of Figure 7 (upper panel). The T_d structure is composed by the original four tetrahedral OH^- groups in the first shell to which three water molecules are added leading to CN = 7, $[Pa(OH)_4(H_2O)_3]^+/T_d$, as in $[PaO_2(H_2O)_5]^+$ and $[PaO(OH)_2(H_2O)_4]^+$. The higher number of first sphere water molecules in $[Pa(OH)_4(H_2O)_3]^+/T_d$ (as compared to $[Pa(OH)_4(H_2O)_2]^+/D_{4h}$) does not especially results on global stabilization on hydration. As we have already shown, the initial tetrahedral symmetry is lost, and it is rearranged into a geometry quite similar to that of the D_{4h} simulation but with an additional water molecule. Both of the Pa−O_{hydr} and Pa−O_w distances are longer than the corresponding D_{4h} ones (the same information comes from the lower and broader RDF peaks).

We now complete the characterization of water hydration structures around Pa(V) and U(VI) by examining the angular distribution functions (ADFs) that provide the tridimensional arrangement of oxygen atoms around the central actinide. In Figure 8A, we show O−An−O ADFs (where An = Pa and U, and

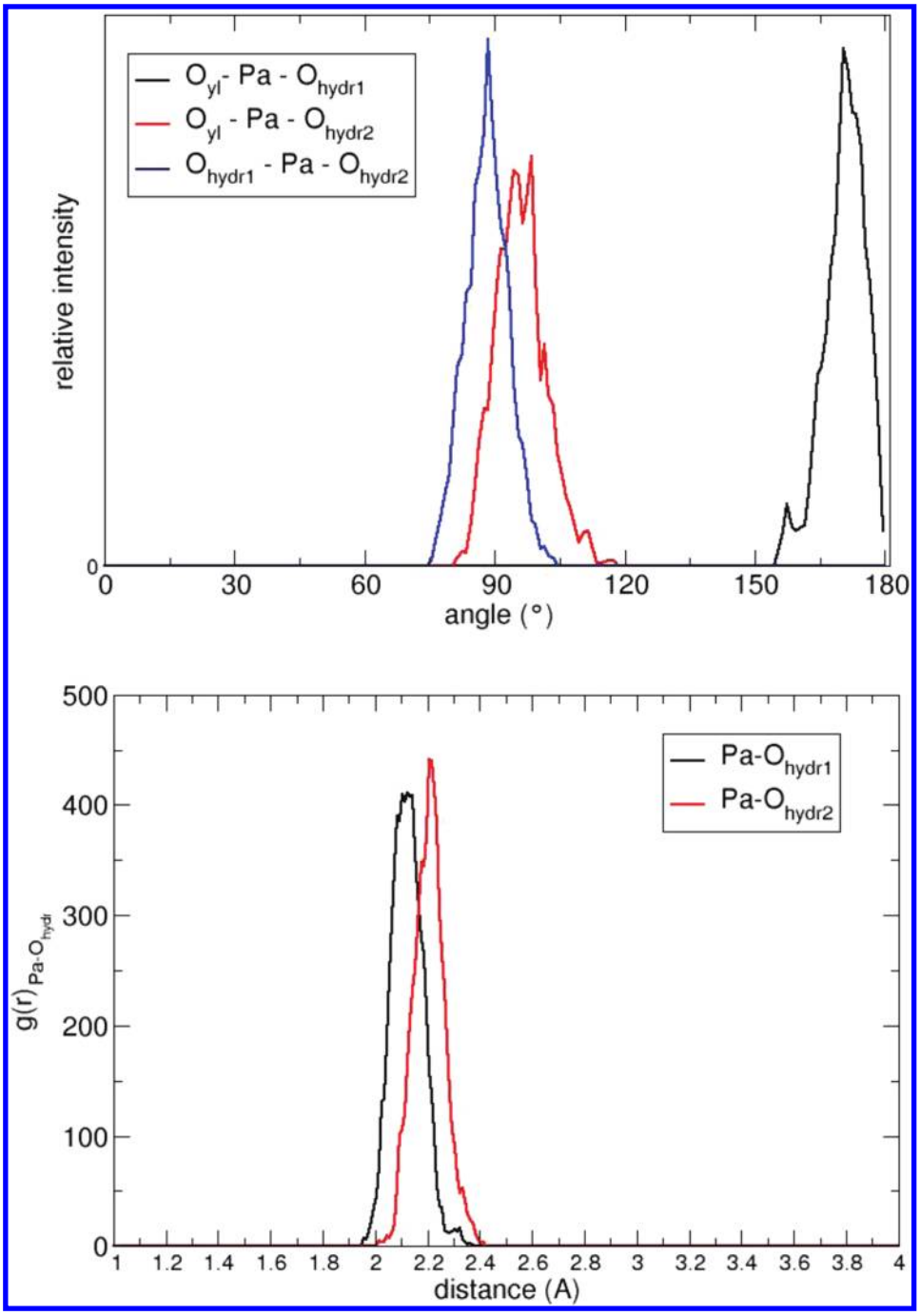

Figure 6. O−Pa−O angular distribution function of the three separated angles of $PaO(OH)_2^+$ simulation (upper panel) and Pa−O_{hydr} radial distribution function where the contribution of the two O_{hydr} atoms is considered separately.

O can be O_{yl}, O_{hydr}, or O of a water molecule). Both hydrated dioxo-cations show very similar ADF shapes with a peak at about 180° corresponding to the characteristic actinyl linear structure formed by the two O_{yl} atoms and the central. PaO_2^+ is slightly less rigid but still linear with a high peak at 90° that corresponds to the angle between the O_{yl} atoms and the water molecules in the equatorial plane. The two other peaks at about 70° and 140° are those formed by the five equatorial water molecules. For $[Pa(OH)_4(H_2O)_2]^+$, we can clearly see the two high peaks characterizing the D_{4h} structure: one at 90° and another one at about 180°. The other isomer, $[Pa(OH)_4(H_2O)_3]^+/T_d$, which has a distorted and not symmetric structure results in a less well-characterized ADF. The high rigidity of water molecules around $Pa(OH)_4^+/D_{4h}$ structure is also clearly shown by the tilting and theta angles presented in Figure 8B and C. All in all, the tilting angles for PaO_2^+ and UO_2^{2+} behave very similarly, although $Pa(OH)_4^+/T_d$ has a less clear signature where $PaO(OH)_2^+$ hydration is in between the highly structured $Pa(OH)_4^+/D_{4h}$ and the low symmetric $Pa(OH)_4^+/T_d$.

3.3. UO_2^{2+} vs PaO_2^+ Water Interaction. We have mentioned earlier the analogies between protactinyl, PaO_2^+, and uranyl, UO_2^{2+}, in water. However, different Pa(V) monocation isomers

dx.doi.org/10.1021/jp111726b |J. Phys. Chem. B 2011, 115, 3560–3570

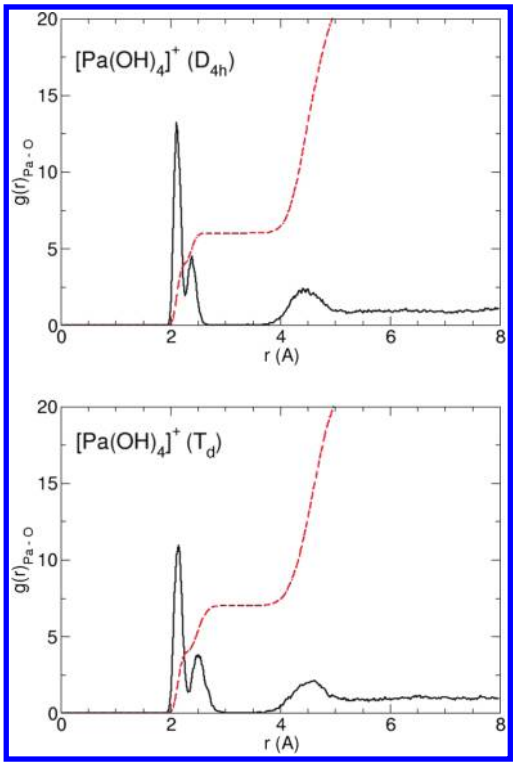

Figure 7. Pa−O radial distribution function, $g(r)$, for the $Pa(OH)_4^+$ simulations: D_{4h} (upper panel) and T_d (lower panel). The dashed line shows the integrated CN.

are stable in water unlike U(VI). We expect that some difference should also reside in the stability and/or structure of PaO_2^+ in water. We have already noticed that the Pa−O bond is slightly longer but this is not a clear indication of what is the cause of the different reactivity, since the change in geometry is expected from the different oxidation states and consequent charge distributions of the two oxo-cations. At this aim, we should better investigate the PaO_2^+ interaction with the surrounding water molecules and compare with UO_2^{2+}.

Before inspecting the molecular details of structure and dynamics of the oxocation−solvent interaction, we first quantify it by monitoring the number of water molecules in the hydration shells. In the first hydration shell, we have seven oxygen atoms around Pa(V) and U(VI). Two of them have short covalent bonds to the actinide (the O_{yl} atoms), while the other five atoms belong water molecules in the equatorial plane. We can then analyze the second hydration shell that is relatively well structured as shown by the second peak of the Pa−O and U−O RDFs (we do not show the U−O RDF but it is similar to what found by previous DFT-based MD simulations[31]). At this end, we show in Figure 9 the probability of having n water molecules in first and second hydration shells. As already noted, the first shell is well-characterized and a constant (and equal between PaO_2^+ and UO_2^{2+}) number of water molecules is present (equal to seven). As usual in cation hydration, the second shell is less structured, but it can still be defined and characterized. As clearly shown in the same Figure 9, PaO_2^+ has much more water molecules in the second hydration shell than UO_2^{2+}. In fact PaO_2^+ has between 15 and 17 water molecules, while UO_2^{2+} has between 12 and 14.[73] This is not a small difference and clearly outside the statistical fluctuations. Simply considering the oxidation states

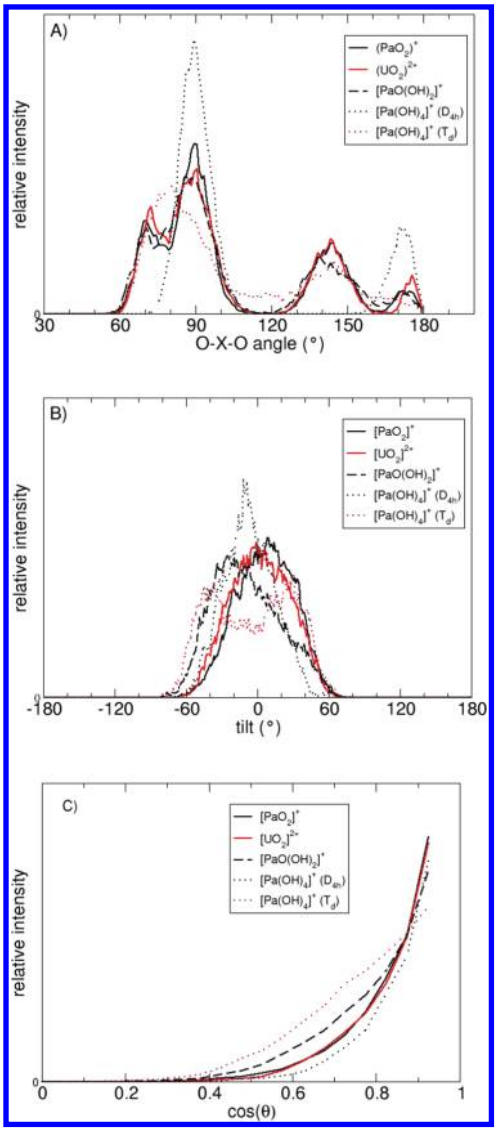

Figure 8. Angular distribution functions between Pa (and U) and first hydration shell water molecules: (A) O−Pa−O, (B) tilting angle, and (C) cosine of θ angle. Angles are defined in section 2.3.

and the charge of the two cations, one could expect that UO_2^{2+}, a dication, should be more attractive for water molecules than PaO_2^+, a monocation, having a similar shape and hindrance. This argument, of course, neglects molecular details that can be crucial to explain why PaO_2^+ has more water molecules in second hydration shell than UO_2^{2+}. To understand this apparently counterintuitive result—i.e. a less charged cation more hydrated than a highly charged similar one—we shall turn to examine hydration details.

The two O_{yl} atoms can interact with water molecules forming what is called apical interaction. The existence and nature of this interaction is a long-standing open question in uranyl hydration. Early MD simulations performed with empirical force fields[29] as well as ab initio calculations in clusters suggested the existence of this interaction.[28,74] On the other hand, MD simulations based on different methods found that the apical interaction is very weak.[30−33] In Figure 10 we show the RDF between O_{yl} atoms and hydrogen atoms of water molecules (H_w) for UO_2^{2+}, PaO_2^+, and $PaO(OH)_2^+$ simulations. In the case of UO_2^{2+} we find the same results as the previous simulations by Bühl et al.[31] where no

dx.doi.org/10.1021/jp111726b |J. Phys. Chem. B 2011, 115, 3560–3570

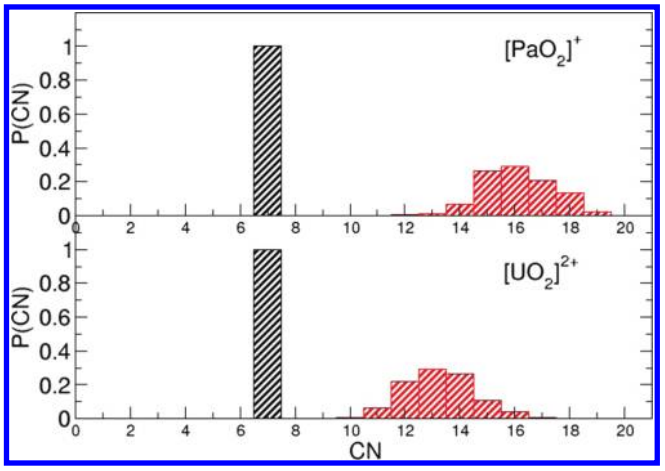

Figure 9. CN probability for the first (black) and second (red) shell. Both O_{yl} and O_w are considered in first shell. The second shell is defined up to the second minimum of Pa−O and U−O $g(r)$ values.

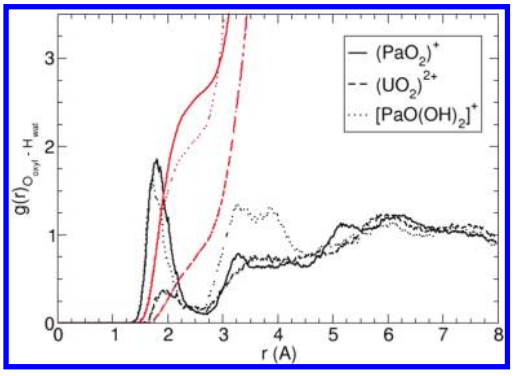

Figure 10. Radial distribution function between O_{yl} atoms and H atoms of water molecules, H_w. The corresponding integrated CNs are also shown in red.

clear apical water molecules were found. We have a small RDF peak with values less than one meaning that only a weak interaction is present and basically no strong H-bonds are formed—and consequently no structural apical water molecules are present. In the case of PaO_2^+, we have a totally different picture. A well-defined peak is present with a coordination number that almost plateaus at 2.5. This means that a clear H-bond network is present around the two O_{yl} atoms of PaO_2^+. A similar picture, but with a slightly less intensity, is found for $PaO(OH)_2^+$, the other Pa(V) species containing an O_{yl} atom.

By using the geometrical H-bond definition of Luzar and Chandler,[75] we can estimate from MD simulations the probability of having an H-bond between the O_{yl} atoms (as an acceptor) and water molecules for the three systems containing O_{yl} atoms. Results are reported in Table 4. It is clearly shown that PaO_2^+ is able to have between two and three H-bonds per O_{yl} atom, whereas UO_2^{2+} has 50% of probability of having no H-bond and it is able to have at most one H-bond. Also the other $PaO(OH)_2^+$ species is able to have more than one H-bond. In general, O_{yl} atoms bound to Pa(V) always form H-bonds, while this is not the case for UO_2^{2+}. The difference of the O_{yl} atoms in forming H-bonds reflects the different partial charges obtained for the two oxocations,[20] showing that O_{yl} of PaO_2^+ are more negatively charged then O_{yl} of UO_2^{2+}. Note that the easiest

Table 4. Probability of Having 3 ($P^{3H\text{-bond}}$), 2 ($P^{2H\text{-bond}}$), 1 ($P^{1H\text{-bond}}$), or 0 ($P^{0H\text{-bond}}$) H-Bonds to the O_{yl} Groups in the PaO_2^+, $PaO(OH)_2^+$, and UO_2^+ CPMD Simulations in Liquid Water

species	$P^{3H\text{-bond}}$	$P^{2H\text{-bond}}$	$P^{1H\text{-bond}}$	$P^{0H\text{-bond}}$
PaO_2^+	0.45	0.45	0.10	0.00
$PaO(OH)_2^+$	0.17	0.56	0.27	0.00
UO_2^+	0.00	0.01	0.53	0.46

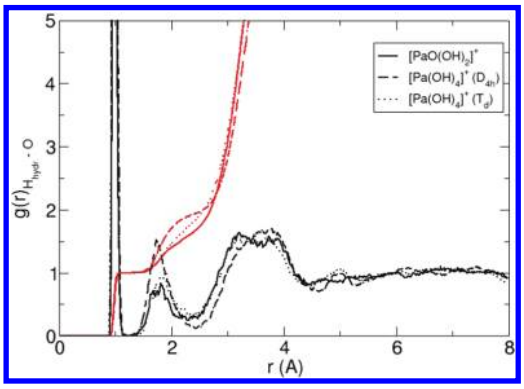

Figure 11. Radial distribution function between H_{hydr} and O atoms. The corresponding integrated CNs are also shown in red.

O_{yl} atoms form H-bonds on hydration, the easiest they should be protonated. Indeed UO_2^{2+} is the less hydrolyzed U(VI) aqueous species, while aqueous Pa(V) monocations can be protonated into $PaOOH^{2+}(aq)$ and possibly even into $PaO^{3+}(aq)$, as discussed in the Introduction.

The tendency of Pa(V) species to form H-bonds in water is also found in hydroxyl species where the oxygen atoms of the hydroxyl groups are able to interact with hydrogen atoms of surrounding water molecules as shown in Figure 11. In particular, the H-bond network is more relevant for $Pa(OH)_4^+/D_{4h}$ species. This capacity of forming short H-bonds in Pa(V) species in water, both apical interaction of PaO_2^+ and $PaO(OH)_2^+$ and H-bonds with O_{hydr} for $PaO(OH)_2^+$ and $Pa(OH)_4^+$ species, suggests that the Pa−O bond (with both O_{hydr} or O_{yl}) is weakened by water solvation. In fact these Pa(V) monocations can be protonated giving dications, like $PaOOH^{2+}$ that is also stable in acid solutions.

4. CONCLUSIONS

By using DFT-based molecular dynamics we were able to point out differences in the chemical behavior of isoelectronic Pa(V) and U(VI) oxo, hydroxo, and mixed oxo-hydroxo cations in noncomplexing aqueous solutions. Namely, Pa(V) covalent isomers of stoichiometries $PaO_2^+(aq)$, $PaO(OH)_2^+(aq)$, and $Pa(OH)_4^+(aq)$ are stable during the simulations, while the U(VI) isoelectronic analogues quickly loose a proton and form the stable $UO_2^{2+}(aq)$ uranyl dioxocation.

The protactinyl dioxocation (PaO_2^+) is able to form a dense H-bond network with two or three H-bonds for each O_{yl} atoms, while UO_2^{2+} is not. Note that gas phase calculations reported apical H-bonds also for UO_2^{2+} and a slight difference—only in distance not in formation—with protactinyl. In clusters, apical water molecules cannot interact properly with bulk molecules

and this is a source of ambiguity in this kind of calculation for the liquid phase. By explicit solvent calculations we found a noticeable difference between the two oxocations abilities to form stable apical interactions.

In particular, comparing PaO_2^+ and UO_2^{2+} simulations in liquid water, we are able to bring some insights into the debate on apical H-bonds for UO_2^{2+} in liquid water. Apical water molecules interact weakly with O_{yl} of UO_2^{2+}, while they interact much more strongly with PaO_2^+ establishing a stable H-bond network. Molecular dynamics was crucial to clearly address such H-bonding in liquid water. This is coherent with static calculations reporting that the O_{yl} atoms of PaO_2^+ are more negatively charged than the equivalent O_{yl} atoms of UO_2^{2+}. This was interpreted as evidence for some intrinsic instability of PaO_2^+ despite similar electronic structures of PaO_2^+ and UO_2^{2+} are stable.[16,20,24,76]

Since apical water molecules can hydrate the O_{yl} sites via H atoms that are slightly positively charged, a more negative charge on O_{yl} atoms can of course increase the interaction between the cation and water molecules. The oxo bond is stronger in UO_2^{2+} than in PaO_2^+ and O_{yl} atoms are less negatively charged, reflecting the tendency of U(VI) in oxocations to form stronger covalent bonds than Pa(V). This might be partially related to the higher atomic charge U(VI), but the more important contribution of 5f orbitals in oxo bonds has also clearly an important role. Another justification can come from a purely electrostatic perspective. PaO_2^+ is a monocation and thus the long-range Coulomb repulsion with partially positively charged H atoms is smaller than from UO_2^{2+} (that is doubly charged); however, this would not explain the difference between Pa(V) and *trans*-protactinian(V) elements of the same charge. This is a relatively long-range and nondirectional phenomenon compared to H-bond to the O_{yl} atoms. However it can play a role in bulk water where there is an interaction balance between forming H-bonds with the O_{yl} atoms and with other water molecules. The large difference noticed between Pa(V) and U(VI) dioxocations can come from a combination of the long- and short-range effects. The differences between in solution and in cluster results on apical water molecules can come from two key differences between gas and condensed phase: (i) H-bond dynamics that is peculiar of liquid character and (ii) even from a structural point of view water molecules in clusters often do not have the choice between interacting with bulk or solute, especially when they are close to the cluster boundary.

Concluding, we can summarize as follows: (i) Pa(V) can form different dioxo, mono-oxo, and hydroxo monocations in water while U(VI) under the same conditions is suddenly transformed in UO_2^{2+}; (ii) Pa(V) behaves differently from U(VI) in water; (iii) There are some similarities in the actinyl oxocations (stable oxo bonds and five well-structured equatorial water molecules); (iv) The ability of forming H-bond network in Pa(V) could be at the basis of its particular water chemistry with respect U(VI) and other transuranium elements that are able to form oxo bonds. These differences between Pa(V) and U(VI) appeared only on careful examination of hydration structure and dynamics, while there were not especially observed in gas phase studies of the bare ions.

AUTHOR INFORMATION

Corresponding Author

*E-mail: riccardo.spezia@univ-evry.fr; pierre.vitorge@cea.fr.

ACKNOWLEDGMENT

We acknowledge GNR-Paris2010 for partial funding. We thank finally GENCI (grant x2010071870) and CEA-CCRT (DSV and DEN) for computing time.

REFERENCES

(1) Silva, R.; Bidoglio, G.; Rand, M.; Robouch, P.; Wanner, H.; Puigdomenech., I. *Chemical Thermodynamics. 2 Chemical Thermodynamics of Americium*; Elsevier: Paris OCDE AEN, 1995.

(2) Grenthe, I.; Fuger, J.; Konings, R.; Lemire, R.; Muller, A.; Nguyen-Trung, C.; Wanner, H. *Chemical Thermodynamics. 1 Chemical Thermodynamics of Uranium*; Wanner, H., I. Forest, Eds.; Elsevier: Paris OCDE AEN, 1992.

(3) Lemire, R.; Fuger, J.; Nitsche, H.; Rand, M.; Spahiu, K.; Sullivan, J.; Ullman, W.; Vitorge, P. *Chemical Thermodynamics. 3 Chemical Thermodynamics of Neptunium and Plutonium*; Elsevier: Paris OCDE AEN, 2001.

(4) Bühl, M.; Schreckenbach, G.; Sieffert, N.; Wipff, G. *Inorg. Chem.* **2009**, *48*, 9977–9979.

(5) Vitorge, P.; Capdevila, H. *Radiochim. Acta* **2003**, *91*, 623–631.

(6) Schreckenbach, G.; Shamov, G. A. *Acc. Chem. Res.* **2010**, *43*, 19–29.

(7) Bühl, M.; Kabrede, H. *ChemPhysChem* **2006**, *7*, 2290–2293.

(8) Spencer, S.; Gagliardi, L.; Handy, N. C.; Ioannon, A. G.; Skylaris, C.-K.; Willetts, A.; Simper, A. M. *J. Phys. Chem. A* **1999**, *103*, 1831–1837.

(9) Buhl, M.; Schreckenbach, G. *Inorg. Chem.* **2010**, *49*, 3821–3827.

(10) Pepper, M.; Bursten, B. E. *Chem. Rev.* **1991**, *91*, 719–741.

(11) Oda, Y.; Aoshima, A. *J. Nucl. Fuel Cycle Environ.* **2002**, *39*, 647–654.

(12) Buhl, M.; Diss, R.; Wipff, G. *J. Am. Chem. Soc.* **2005**, *127*, 13506–13507.

(13) Shamov, G. A.; Schreckenbach, G. *J. Phys. Chem. A* **2005**, *109*, 10961–10974.

(14) Gutowski, K. E.; Dixon, D. A. *J. Phys. Chem. A* **2006**, *110*, 8840–8856.

(15) Siboulet, B.; Marsden, C. J.; Vitorge, P. *Chem. Phys.* **2006**, *326* (2−3), 289–296.

(16) Straka, M.; Dyall, K.; Pyykkö, P. *Theor. Chem. Acc.* **2001**, *106*, 393–403.

(17) Guillaumont, R.; Bouissieres, G.; Muxart, R. *Actinides ReV.* **1968**, *1*, 135.

(18) Vitorge, P.; Capdevila, H.; Maillard, S.; Fauré, M.-H.; Vercouter, T. *J. Nuclear Sc. Techno.* **2002**, No. Supplement 3, 713–716.

(19) Vitorge, P.; Phrommavanh, V.; Siboulet, B.; You, D.; Vercouter, T.; Descostes, M.; Marsden, C. J.; Beaucaire, C.; Gaudet, J. P. *C. R. Acad. Sci., Ser. IIb: Chim.* **2007**, *10*, 978–993.

(20) Siboulet, B.; Marsden, C. J.; Vitorge, P. *New J. Chem.* **2008**, *32* (12), 2080–2094.

(21) Brown, D.; Maddock, A. G. Analytical Chemistry. In *Progress in Nuclear Energy*; Pergamon press; Oxford & New York, 1967.

(22) Muxart, R.; Guillaumont, R. Protactinium. In *Compléments au Nouveau Traité de Chimie minérale*; Masson: Paris, 1974.

(23) Myasoedov, B.; Kirby, H. W.; Tananaev, I. G. Protactinium. In *The Chemistry of the Actinide and Transactinide Elements*; Springer: The Netherlands, 2006.

(24) Toraishi, T.; Tsuneda, T.; Tanaka, S. *J. Phys. Chem. A* **2006**, *110*, 13303–13309.

(25) Santos, M.; Pires de Matos, A.; Marçalo, J.; Gibson, J. K.; Haire, R. G.; Tyagi, R.; Pitzer, R. M. *J. Phys. Chem. A* **2006**, *110*, 5751–5759.

(26) Le Naour, C.; Trubert, D.; Di Giandomenico, M. V.; Fillaux, C.; Den Auwer, C.; Moisy, P.; Hennig, C. *Inorg. Chem.* **2005**, *44*, 9542–9546.

(27) Mendes, M.; Hamadi, S.; Le Naour, C.; Roques, J.; Jeanson, A.; Den Auwer, C.; Moisy, P.; Topin, S.; Aupiais, J.; Hennig, C.; Di Giandomenico, M.-V. *Inorg. Chem.* **2010**, *49*, 9962–9971.

(28) Schreckenbach, G.; Shamov, G. A. *Acc. Chem. Res.* **2010**, *43*, 19–29and references therein..
(29) Guilbaud, P.; Wipff, G. *J. Phys. Chem.* **1993**, *97*, 5685–5692.
(30) Hagberg, D.; Karlström, G.; Roos, B. O.; Gagliardi, L. *J. Am. Chem. Soc.* **2005**, *127*, 14250–14256.
(31) Bühl, M.; Kabrede, H.; Diss, R.; Wipff, G. *J. Am. Chem. Soc.* **2006**, *128*, 6357–6368.
(32) Nichols, P.; Bylaska, E. J.; Schenter, G. K.; de Jong, W. *J. Chem. Phys.* **2008**, *128*, 124507.
(33) Frick, R. J.; Hofer, T. S.; Pribil, A. B.; Randolf, B. R.; Rode, B. M. *J. Phys. Chem. A* **2009**, *113*, 12496–12503.
(34) Den Auwer, C.; Guillaumont, D.; Guilbaud, P.; Condradson, S. D.; Rehr, J. J.; Ankudinov, A.; Simoni., E. *New J. Chem.* **2004**, *28*, 929–933.
(35) Allen, P. G.; Bucher, J. J.; Shuh, D. K.; Edelstein, N. M.; Reich, T. *Inorg. Chem.* **1997**, *36*, 4676–4683.
(36) Bolvin, H.; Wahlgren, U.; Gropen, O.; Marsden, C. J. *J. Phys. Chem. A* **2001**, *105*, 10570–10576.
(37) Bernasconi, L.; Blumberger, J.; Sprik, M.; Vuilleumier, R. *J. Chem. Phys.* **2004**, *121*, 11885.
(38) Ayala, R.; Sprik, M. *J. Chem. Theory Comput.* **2006**, *2*, 1403–1415.
(39) Bühl, M.; Grigoleit, S.; Kabrede, H.; Mauschick, F. T. *Chem.—Eur. J.* **2006**, *12*, 477–488.
(40) Amira, S.; Spangberg, D.; Zelin, V.; Probst, M.; Hermansson, K. *J. Phys. Chem. B* **2005**, *109*, 14235–14242.
(41) Yazyev, O. V.; Helm, L. *Theor. Chem. Acc.* **2006**, *115*, 190–195.
(42) Marx, D.; Hutter, J.; Parrinello, M. *Chem. Phys. Lett.* **1995**, *241*, 457–462.
(43) Tuckerman, M. E.; Laasonen, K.; Sprik, M.; Parrinello, M. *J. Phys. Chem.* **1995**, *99*, 5749–5752.
(44) Hunt, P.; Sprik, M. *ChemPhysChem* **2005**, *6*, 1805–1808.
(45) Heuft, J. M.; Meijer, E. J. *J. Chem. Phys.* **2005**, *122*, 094501.
(46) Terrier, C.; Vitorge, P.; Gaigeot, M.-P.; Spezia, R.; Vuilleumier, R. *J. Chem. Phys.* **2010**, *133*, 044509.
(47) Yazyev, O. V.; Helm, L. *J. Chem. Phys.* **2007**, *127*, 084506.
(48) Pollet, R.; Marx, D. *J. Chem. Phys.* **2007**, *126*, 181102.
(49) Ayala, R.; Spezia, R.; Vuilleumier, R.; Martinez, J. M.; Pappalardo, R. R.; Sanchez Marcos, E. *J. Phys. Chem. B* **2010**, *114*, 12866–12874.
(50) Car, R.; Parrinello, M. *Phys. Rev. Lett.* **1985**, *55*, 2471–2474.
(51) Troullier, N.; Martins, J. L. *Phys. Rev. B* **1991**, *43*, 1993–2006.
(52) Kleinman, L.; Bylander, D. M. *Phys. Rev. Lett.* **1982**, *48*, 1425–1428.
(53) Spezia, R.; Tournois, G.; Tortajada, J.; Cartailler, T.; Gaigeot, M.-P. *Phys. Chem. Chem. Phys.* **2006**, *8*, 2040–2050.
(54) Spezia, R.; Duvail, M.; Vitorge, P.; Cartailler, T.; Tortajada, J.; Chillemi, G.; D'Angelo, P.; Gaigeot, M.-P. *J. Phys. Chem. A* **2006**, *110*, 13081–13088.
(55) Bresson, C.; Spezia, R.; Esnouf, S.; Solari, P. L.; Coantic, S.; Den Auwer, C. *New J. Chem.* **2007**, *31*, 1789–1797.
(56) Spezia, R.; Bresson, C.; Den Auwer, C.; Gaigeot, M.-P. *J. Phys. Chem. B* **2008**, *112*, 6490–6499.
(57) Ismail, N.; Heully, J. L.; Saue, T.; Daudey, J. P.; Marsden, C. J. *Chem. Phys. Lett.* **1999**, *300*, 296–302.
(58) Bouteiller, Y.; Mijoule, C.; Nizam, M.; Barthelat, J. C.; Daudey, J. P.; Pelissier, M.; Silvi, B. *Mol. Phys.* **1988**, *65*, 295.
(59) Dunning, T. H. ; Hay, P. J. *Modern Theoretical Chemistry 3*; Schaefer, H. F., Ed.; Plenum: New York, 1977.
(60) Becke, A. D. *J. Chem. Phys.* **1993**, *98*, 5648.
(61) Becke, A. D. *Phys. Rev. A.* **1988**, *38*, 3098–3100.
(62) Miehlich, B.; Savin, A.; Stoll, H.; Preuss, H. *Chem. Phys. Lett.* **1989**, *157*, 200–206.
(63) Lee, C.; Yang, W.; Parr, R. G. *Phys. Rev. B* **1988**, *37*, 785–789.
(64) Hutter, J.; Alavi, A.; Deutsch, T.; Bernasconi, M.; Goedecker, S.; Marx, D.; Tuckerman, M.; Parrinello, M. *CPMD*, version 3.9.1; IBM Research Division, IBM Corp and Max Planck Institute: Stuttgart, 2004.
(65) Frisch, M. J.; et al. *Gaussian 03*, revision D.01; Gaussian, Inc.: Wallingford, CT, 2004.
(66) Wahlgren, U.; Moll, H.; Grenthe, I.; Schimmelpfennig, B.; Maron, L.; Vallet, V.; Gropen, O. *J. Phys. Chem. A* **1999**, *103*, 8257–8264.
(67) Clark, D. L.; Conradson, S. D.; Donohoe, R. J.; Webster Keogh, D.; Morris, D. E.; Palmer, P. D.; Rogers, R. D.; Tait, C. D. *Inorg. Chem.* **1999**, *38*, 1456–1466.
(68) Schreckenbach, G.; Hay, P. J.; Martin, R. L. *Inorg. Chem.* **1998**, *37*, 4442–4451.
(69) Bühl, M.; Schreckenbach, G. *Inorg. Chem.* **2010**, *49*, 3821–3827.
(70) Note that these out-of-equilibrium results should be taken as a trend. In the real solution, the pH is often buffered and it guides the equilibrium. What we like to underline here is that in the case of U(VI) there is a clear driving force towards the formation of the dioxocation, such that if the UO bond is not present, the OH^- groups bound to U(VI) tend to lose a proton. Another case is the uranyl in basic media where the OH^- groups are bound to the U but replacing the equatorial water molecules. Structure and stabilities of these compounds are well discussed in other works.[66−69]
(71) Here we cannot talk of same pH, since we do not control it, but we have the same conditions in the sense of same initial structures, particles, number of electrons, and number of solvent water molecules. In this sense, the conditions are the same for each couple and the differences are to be taken into account system by system.
(72) Shannon, R. D. *Acta Crystallogr.* **1976**, *A32*, 751–767.
(73) We should notice that the second hydration shell of UO_2^{2+} obtained by our DFT-based molecular dynamics is very similar to that reported by a recent HF/MM simulation.[33]
(74) Calculations in clusters, even including more than first hydration shell have intrinsic ambiguities in determining the existence of an apical bond. In fact in bulk water, a molecule is in competition between being hydrogen bonded with the oxo atoms or with oxygen atoms of the bulk. The bulk not being present in cluster calculations excludes this latter choice such that the apical bond is the only possible interaction.
(75) Luzar, A.; Chandler, D. *Nature* **1996**, *379*, 55–57.
(76) Kaltsoyannis, N. *Inorg. Chem.* **2000**, *39*, 6009–6017.